SYNTHESIS AND CHARACTERiZATION OF $ABi_4Ti_4O_{15}$ (A=Sr,Ba,Ca) CERAMIC

A THESIS

Submitted by

Kuntal Mitra

Roll no.-413PH2088

Under the guidance of

Prof. S. Panigrahi

Department of Physics and Astronomy

National Institute of Technology, Rourkela

NATIONAL INSTITUTE OF TECHNOLOGY

ROURKELA

CERTIFICATE

This is to certify that the thesis titled "SYNTHESIS AND CHARACTERiZATION OF $ABi_4Ti_4O_{15}$ (A=Sr,Ba,Ca) CERAMIC" submitted by Mr. Kuntal Mitra in partial fulfillments for the requirements for the award of Master of Science Degree in Physics Department at National Institute of Technology, Rourkela is an genuine work carried out by him under my supervision and guidance. To the best of my knowledge, the matter embodied in the project has not been submitted to any other University/ Institute for the award of any Degree or Diploma.

Rourkela-769008

Prof.S.Panigrahi

Dept of Physics and Astronomy

DECLARATION OF THE CANDIDATE

I hereby declare that the project work entitled "SYNTHESIS AND CHARACTERISATION OF $ABi_4Ti_4O_{15}$ (A=Sr,Ba,Ca) CERAMIC " is an authentic work carried by me, during the one year project at NIT, Rourkela, from July 2014 to May 2015 under the supervision of PROF.S.PANIGRAHI and is being submitted for the partial fulfillment of the requirement for award of the degree of Master of Science in Physics to NIT, Rourkela. This has not been submitted anywhere else for the award of any other degree.

Date: Kuntal Mitra

ACKNOWLEDGEMENTS

Before presenting the thesis work, I would like to mention a few words for the people who gave their complete support for my thesis work.

My first thanks are to the Almighty God, without whose blessings I wouldn't have been writing this “acknowledgments”. Then I take this opportunity to express my deep regards and sincere gratitude for this valuable, expert guidance rendered to me by guide Prof. S. Panigrahi, Department of Physics, National Institute of Technology Rourkela. I consider me fortunate to have had opportunity to work under his guidance and enrich myself from his vast knowledge and analysis power.

My sincere thanks to Dr. D.K. Bisoyi, Professor and Head of Physics Department for his talented advice and providing necessary facility for my work. I am especially indebted to Priyambada Nayak, for teaching me both research and writing skills, which have been proven beneficial for my current research and future career. Without his endless efforts, knowledge, patience, and answers to my numerous questions, this research would have never been possible.

My deep sense of gratitude to PhD Scholar, Rakesh Muduli and Ranjit Pattanayak department of Physics, for his valuable suggestions and constant help for this work. He has been very kind and patient while suggesting me the outlines of this project and has clarified all my doubts whenever I approached him. I record my sincere thanks to Department of Ceramic Engineering,(NIT Rourkela) for extending all facilities to carry out the FESEM and Department of Physics, (St. Xavier’s College,Ranchi) for their support on doing FTIR spectroscopy. I am greatly thankful to all the research scholars of the department and my class mates for their inspiration and help.

Last but not the least; I would like to express my gratefulness to my parents for their endless support, without which I could not complete my project work.

Date: Kuntal Mitra

CONTENT

ABSTRACT

The report presents the synthesis and characterization of $ABi_4Ti_4O_{15}$ (A=Sr,Ba,Ca) ceramics.The samples are prepared by conventional solidstate reaction route. The room temperature X-ray diffraction study revealed that the compounds were having orthorhombic symmetry. Williamson and Hall equation was used to determine the microstrain ,the particle size and the dislocation density. The SEM micrograph shows plate like grains and the grain size are calculated. Temperature dependent dielectric study showed normal ferroelectric to paraelectric transition in SBT and CBT compound where as relaxor like behavior near phase transition. The Ferroelectric behavior were studied by hysteresis loop. The optical band gap are found to be 3.17 eV , 3.03 eV and 2.84 eV for SBT, BBT and CBT ceramic which is measured from the UV–Visible spectroscopy study.

CHAPTER – 1

INTRODUCTION

1.1 Dielectric Phenomena:

A material which is a poor conductor of electricity, but efficient to electrostatic fields are known as Dielectric materials. The most important property of these materials are they support the support the electric field with a minimum loss of energy in the form of heat. The lower the energy lost as heat (dielectric loss), the more effective is a dielectric material. Another factor is the dielectric constant , i.e. the property of concentrating the electrostatic field lines. Materials with low dielectric constant includes a perfect vacuum, dry air and gases such as helium and nitrogen. Materials with moderate dielectric constants include ceramics, distilled water, glass, mica, paper and polyethylene. Metal oxides, generally, have high dielectric constants.

The materials with high dielectric constant can be used for storing high value of capacitance within a small volume. But if the potential across a dielectric material becomes too high, the material will starts conducting current. This is known as dielectric breakdown.

The dielectric constant is the ratio of the capacitance of a capacitor containing the dielectric to that of an identical but empty capacitor.

Dielectric constant can also be defined in terms of the permittivity of the material. The effect of a material on an electric field is known as the permittivity, the higher the permittivity, the more the material tends to reduce any field set up in it. Since the dielectric material reduces the field by becoming polarized, an entirely equivalent definition is that the permittivity expresses the ability of a material to polarize in response to an applied field. The dielectric constant (sometimes called the 'relative permittivity') is the ratio of the permittivity of the dielectric to the permittivity of a vacuum, so the greater the polarization developed by a material in an applied field of given strength, the greater the dielectric constant will be.

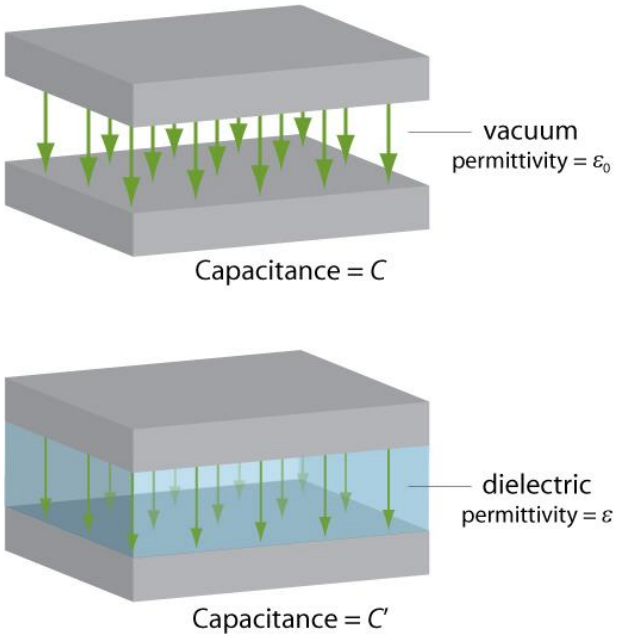

FIGURE-1

The two definitions of the dielectric constant are illustrated by the diagram(the green arrows represent the electric field).

$$\kappa = C'/C \qquad \kappa = \varepsilon/\varepsilon_0$$

All crystalline dielectrics in which polarization or electric dipole moment can be induced by the application of external electric field , are divided in to two classes:

- Polar (dipole) dielectrics.
- Non-polar (neutral) dielectrics.

In polar (dipole) dielectrics, a permanent polarization (Ps) exists even in the absence of applied electric field. In the case of non-polar dielectrics, there is no such permanent polarization.[1]

1.1.2. DIFFERENT TYPES OF POLARIZATION

There are four different types of polarizations:

- Electronic Polarization (P_e) which occurs due to alteration of the electron density.
- Atomic or Ionic polarization (P_i) which is due to ionic charge elastic deformation.
- Orientation Polarization (P_o) which is due to the transformation in orientation of permanent dipole moments
- Space charge polarization due to spatial split-up of charges with in the material.

DIELECTRIC SPECTROSCOPY

Dielectric spectroscopy is the measure of the dielectric properties of a medium as a function of frequency. It is based on the interaction of an external field with the electric dipole moment of the sample, often expressed by permittivity.

It is also an experimental method of characterizing electrochemical systems. This technique measures the impedance of a system over a range of frequencies.

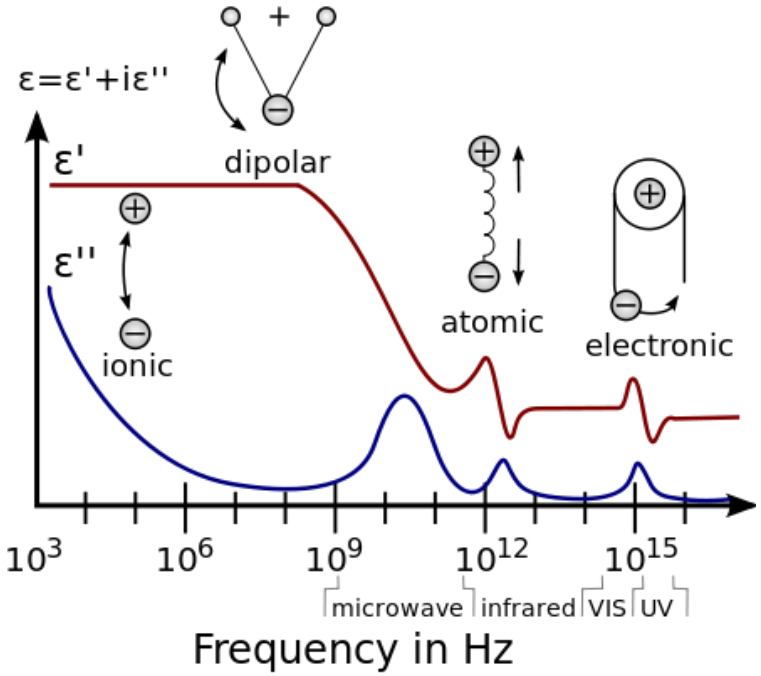

An illustration of the frequency response of various dielectric mec hanisms in terms of the real and imaginary parts of the permittivity.

1.1.3 Piezoelectricity:

Piezoelectric Effect is the ability of certain materials to generate an electric charge in response to applied mechanical stress. The word Piezoelectric is derived from the Greek piezein, which means to squeeze or press, and piezo, which is Greek for “push”.

This is the property of certain materials by virtue of which on applying mechanical stress leads to a generation of electric signals. This can also occur conversely known as converse piezoelectric effect where a electric signals lead to generation of mechanical stress.

These materials are commonly used in STM probe head to detect the morphology. Mostly we can see the use of these materials in lighters.

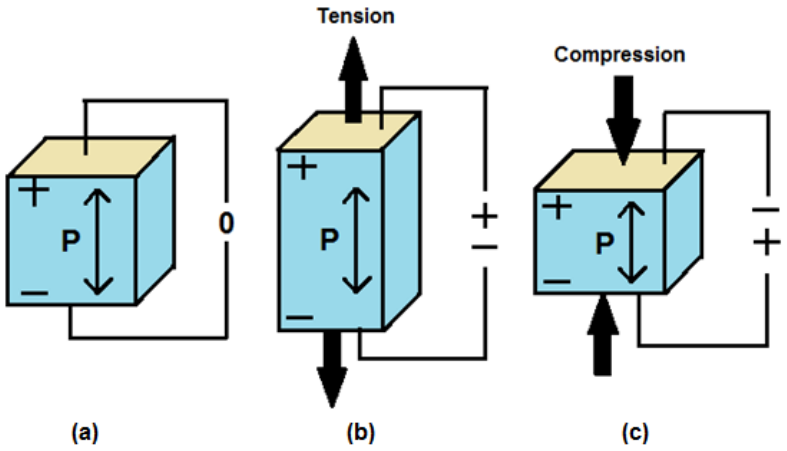

Schematic of direct piezoelectric effect;

(a) Piezoelectric material

(b) Energy generation due to tension

(c) Energy generation due to compression

1.1.4 Pyroelectricity:

Pyroelectricity is the property of some dielectric materials which gets polarized on changing the temperature. This is a subgroup of Piezoelectric material where 10 fall into the category of pyroelectric. These are further sub divided into ferroelectricity.

1.1.5 Ferroelectricity:

Ferroelectricity, property of certain nonconducting crystals, or dielectrics, that exhibit spontaneous electric polarization (separation of the centre of positive and negative electric charge, making one side of the crystal positive and the opposite side negative) that can be reversed in direction by the application of an appropriate electric field. Ferroelectricity is named by analogy with ferromagnetism, which occurs in such materials as iron. Iron atoms, being tiny magnets, spontaneously align themselves in clusters called ferromagnetic domains, which in turn can be oriented predominantly in a given direction by the application of an external magnetic field.

1.2 Basis of Ferroelectricity:

Ferroelectric materials have captivated scientists since their discovery in 1920 [1,2]. In relationship with ferromagnets, the typical properties of ferroelectrics include spontaneous electric polarization, disappearance of the polarization above a ferroelectric phase transition temperature T_c and

polarization reversal. Ferroelectric materials have been a productive field for the study of phase transitions, electron–phonon interactions, Polari tons, and other optical and electrical phenomena in condensed matter.

These materials are characterized by high dielectric constant, piezoelectric coefficient and pyroelectric coefficient.. In solid state physics, ferroelectricity is often deduced as phenomena of network subtleties or as shuddering of phonons. In solid state chemistry, the methods are much closer to the demesne of crystallography than to that of spectroscopy. The polar chattels of conventional ferroelectrics become apparent only below temperature T_c termed the Curie temperature. The high temperature state is referred to as being paraelectric. A ferroelectric crystals are composed of domains in which polarization occurs homogeneously in the same direction.

1.2.1 Hysterisis loop

The domain structure effects several non-linear properties of such substances, among which there is the non-linear dependency of the electrical polarization on the exterior field $P = P(E)$

The image below shows the hysteresis curves of a ferroelectric substance, which proves that the effect of an external electrical field causes the relocation of domains. The different rates at which the domains and the electrical field change lead to a phase difference between the electric field intensity and the polarization, hence the non-linear variations. The loop never retraces the same path. The curve begins with the virgin curve up to a saturation value of polarization. Then decreasing the electric potential to zero there is some remnant polarization. The polarization decreases to zero at a critical value of electric potential.

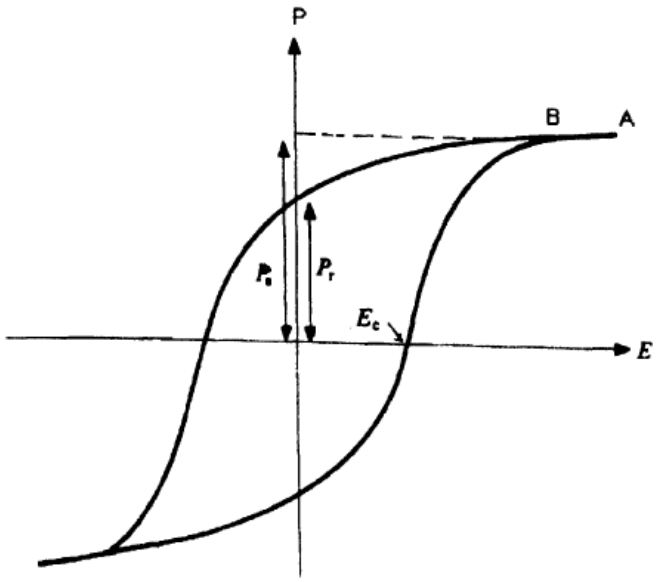

Ferroelectric hysteresis loop (polarization vs. applied voltage)

P_r – remnant polarization

P_s – saturation polarization

E_c – critical value for electric field

More is the remnant polarization the more it is useful as memory element.

1.2.2 Phase transition

The ferroelectric properties of a ferroelectric vanishes above a critical temperature T_c; this temperature is called the ferroelectric Curie temperature. Above this temperature the material is said to be at paraelectric state. The figure shows three major phase transitions.

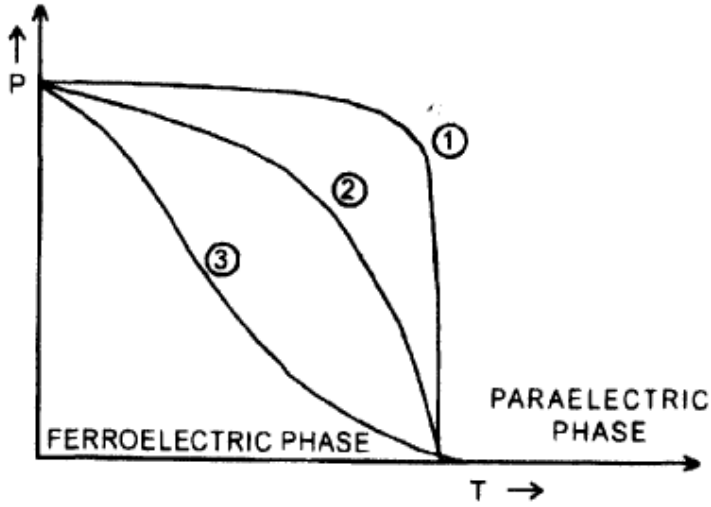

Polarisation as a function of temperature for ferroelectrics:

1. First order
2. Diffuse phase transition
3. Second order

The transition from ferroelectric state to paraelectric state is said to be first order if it is discontinuous i.e. if Ps acquires a zero value immediately at T_c and second order if it is continuous, i.e. if Ps decreases continuously from maximum to zero as T approaches Tc [3]. It should be mentioned that the spontaneous polarization in ferroelectric state is associated with spontaneous electrostrictive strain in the crystal. Thus ferroelectric structure has a lower symmetry than that of paraelectric state [4, 5]. At the transition temperature, a change in crystal structure is therefore observed.

The primary feature of ferroelectric is the anomalous dependence of the dielectric constant on temperature. The dielectric constant temperature diagrams for a fernelectric has one or more very sharp maxima where E can reach values of several thousands. The temperatures at which these maxima occur are called Curie temperatures. Above the Curie temperature ε obeys the Curie Weiss law [6]

$$\varepsilon = \frac{c}{(T - \theta)} + \varepsilon_o$$

where C is a constant and ɵ is a characteristic temperature which is usually some degrees smaller than the transition temperature Tc, ε, is a constant contributed by the electronic polarization. In the vicinity of the transition temperature, ε_o may be neglected since it is of the order of unity and

$$\varepsilon \gg \varepsilon_o$$

Many phase transitions in macroscopic homogeneous materials are characterized by the fact that the transition temperature is not sharply defined. In these, so-called diffuse phase transition temperature (DPT), the transition is smeared out over a certain temperature interval, resulting in a gradual change of physical properties in this temperature region. Though this phenomenon is observed in several types of materials , however, the most remarkable examples of DPT are found in ferroelectric materials . Ferroelectrics diffuse phase transitions (FDPT) are first mentioned in the literature in the early 1950's. Some characteristics of the DPT are [7-9]:

- Broadened maxima in the permittivity- temperature curve,
- Gradual decrease of spontaneous and remanent polarisations with rising temperature,
- Transition temperatures obtained by different techniques which do not coincide,
- Relaxation character of the dielectric properties in transition region
- No Curie-Weiss behavior in certain temperature intervals above the transition temperature.

1.2.3 Types of ferroelectric material

Ferroelectrics material can be classified as two types basing on its transition from ferroelectric to paraelectric behaviour, such as

1) Normal ferroelectric
2) Relaxor ferroelectric

- **Normal ferroelectric materials**: These type of material are characterized by sharp phase transition at curie point depends feebly on frequency. They are following curie-Weiss law. Mostly they have high remnant polarization, behave anisotropically with light.

- **Relaxor ferroelectric materials**: These type of materials are characterized by broad diffused phase transition and are strongly responding the changes in

frequency. They follow Curie-Weiss square law. Mostly possess low remnant polarization and have weak anisotropic behavior with light

STURCTURAL CLASSIFICATION OF Ferroelectric MATERIAL

1. Pervoskite structure

2. Tungsten-Bronze structure

3. Pyrochlore structure

4. Bismuth layered structure

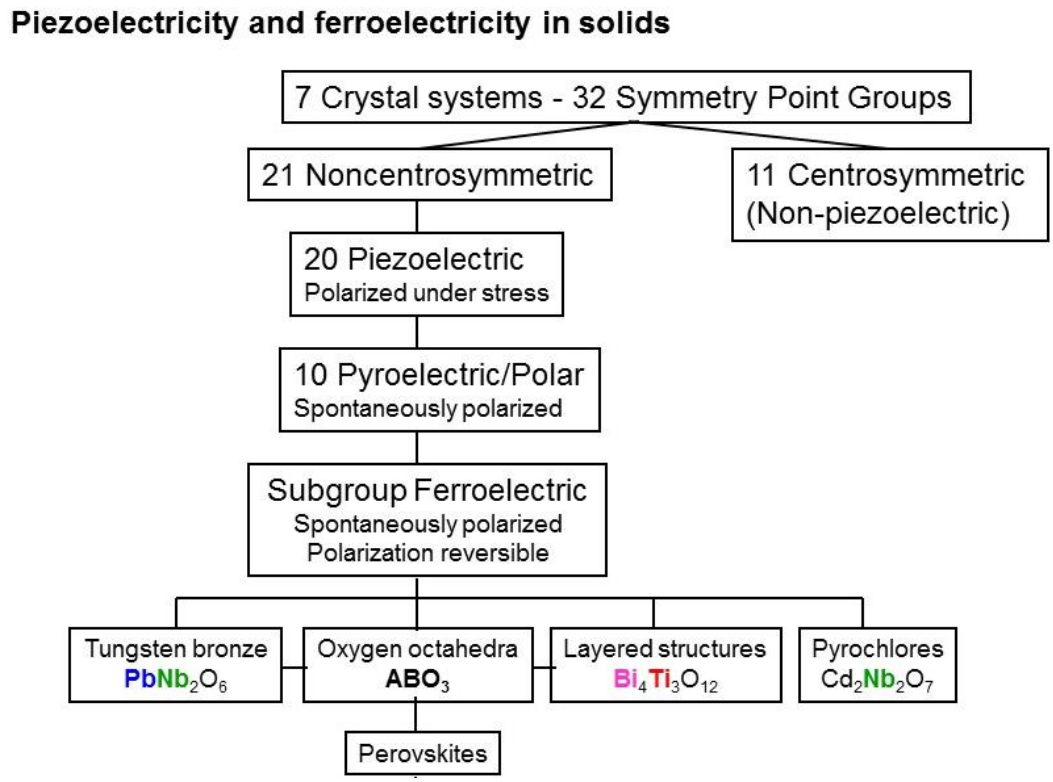

Pervoskite structure

The perovskite structure has the general stoichiometry ABO_3, where "A" and "B" are cations and "O" is an anion. The A cation is divalent and the B cation is tetravalent.[10]

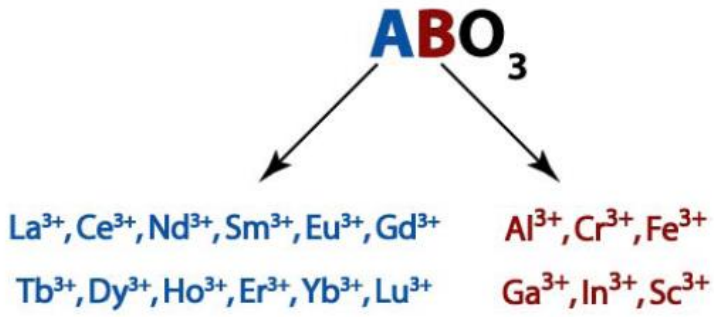

The ions occupying the A and B lattice sites.

The traditional view of the perovskite lattice is that it consists of small B cations within oxygen octahedra, and larger A cations which are XII fold coordinated by oxygen.

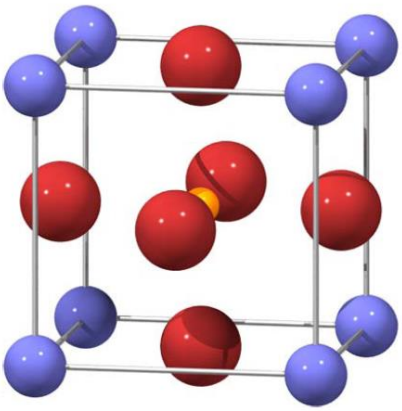

The structure of an ideal cubic perovskite where the A cations are shown at the corners of the cube, and the B cation in the centre with oxygen ions in the face-centred positions

The spacegroup for cubic perovskites is Pm3m (221) [102]; the equivalent positions of the atoms are detailed in Table [11].

Site	Location	Co-ordinates
A cation	(2a)	$(0, 0, 0)$
B cation	(2a)	$(\frac{1}{2}, \frac{1}{2}, \frac{1}{2})$
O anion	(6b)	$(\frac{1}{2}, \frac{1}{2}, 0)$ $(\frac{1}{2}, 0, \frac{1}{2})$ $(0, \frac{1}{2}, \frac{1}{2})$

Atomistic positions in cubic perovskites

Tungsten-Bronze structure

$A1A2_2B1B2_4O_{15}$ is the general formula of a tungsten bronze type structure. The tungsten bronze structure consists of a network of corner sharing BO_6 octahedral with A cations located in interstitial sites. The A1 site is a 12- coordinate site and the A2 site is a larger 15-coordinate site. Combined with a smaller, unoccupied, 9-coordinate C site, these A and C sites form channels through the structure running along the c-direction. Tungsten bronze type compounds have been shown to display industrially significant properties, finding use in volatile memory, actuators, infrared radiation detection as well as in optical applications amongst others.

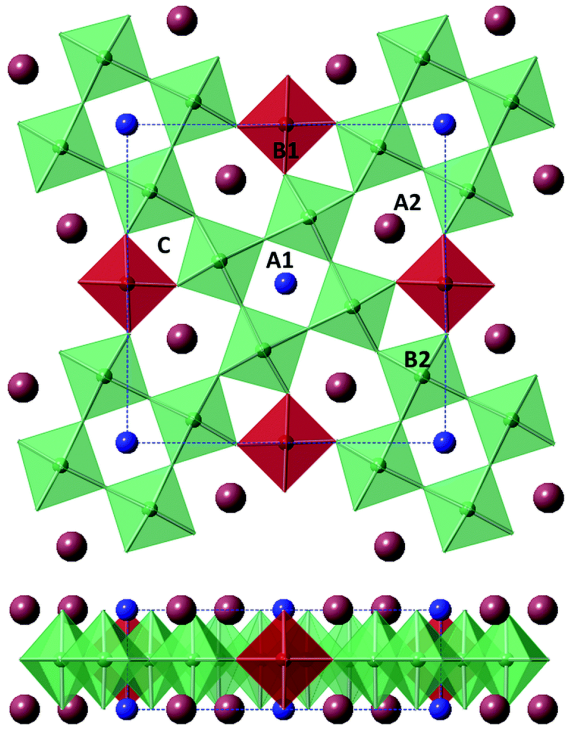

Tungsten-Bronze structure

Pyrochlore

Pyrochlore is also a more general term for the pyrochlore crystal structure (Fd-3m). The more general crystal structure defines materials of the type $A_2B_2O_6$ and $A_2B_2O_7$ where the A and B classes are generally rare-earth or transition metal classes; e.g. $Y_2Ti_2O_7$. The additional anion

vacancy resides in the tetrahedral interstice between adjacent B-site cations. These systems are particularly susceptible to geometrical frustrationand novel magnetic effects [14].

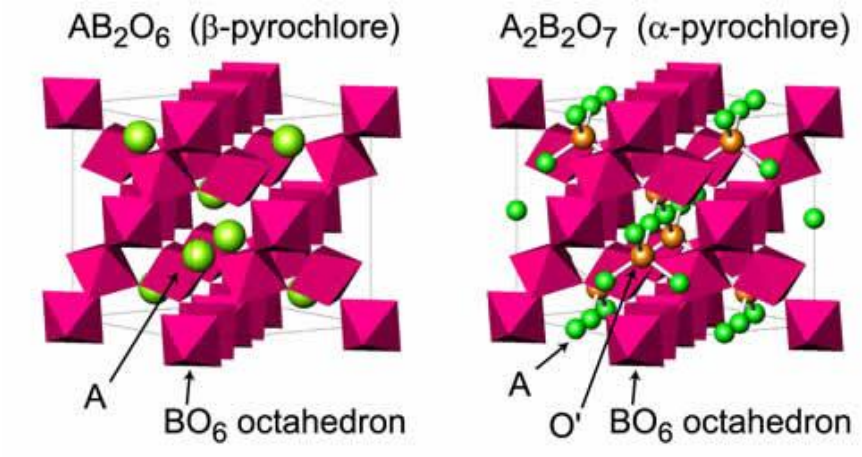

Pyrochlore structures

Bismuth layered structure

Bismuth layer structured ferroelectrics (abbreviated as BLSFs) have fascinated considerable attention for their potential applications in non-volatile random access memory (NVRAM) and high temperature piezoelectric devices. The generic chemical formula for BLSFs is $(Bi_2O_3)^{2+}$ $(A_{m-1}B_mO_{3m+1})^{2-}$, where A is mono-, di- or trivalent cations (e.g., Na^+ , K^+ Ba^{2+} , Ca^{2+} , Pb^{2+} or Bi^{3+}), B is tetra-, penta- or hexavalent cations of a transition metal (e.g., Ti^{4+} , Nb^{5+} ,Ta^{5+} ,or W^{6+}), and m is the number of perovskite-like layers (m = 1,2, 3, 4, 5) [15-17] . The crystal structure of these compounds is composed of $(Bi_2O_2)^{2+}$ layers interleaved with perovskite like blocks $(A_{m-1}B_mO_{3m+1})^{2-}$.

CHAPTER – 2

LITERATURE REVIEW

Introduction:

In recent years FERROELECTRIC materials have acknowledged great consideration for their use in the nonvolatile ferroelectric random access memory (FeRAM) and storage devices. Among these ferroelectrics with lead-based materials have been studied extensively due to their high dielectric constant, piezoelectric coefficient, large remnant polarization (P_r)moderately low coercive field (E_c), and high Curie temperature. However, these ferroelectric materials suffer serious polarization fatigue complications and also have drawbacks considering the environmental issue. Therefore, it is necessary to develop environmentally-friendly lead-free material and output becomes sensitive. With this interest Bismuth-layered perovskite material possesses an important position because of its good ferroelectric properties, including, low coercive field, moderate remnant polarization, long retention, and low tendency to imprint high fatigue resistance with the ability to withstand 10^{12} erase/ rewrite operations [18]. These excellent properties make the Bismuth-layered perovskite materials a very attractive candidate for nonvolatile FeRAM application and high temperature piezoelectric sensors [19].

a) It is well known that the most popular ferroelectric material for non volatile memory applications is $PbZr_xTi1_xO_3$ (PZT), due to their high Curie temperature and large remnant polarization [20]. In spite of these properties, these materials have serious fatigue degradation problems, which can be solved by changing the electrode. Due to the above characteristics bismuth layer structure ferroelectric material are the alternative material. The structure of BLSF comprises of intergrowth of $(Bi_2O_2)^{2+}$ units and pseudo-perovskite slabs $(A_{n-1}B_nO_{3n+1})^{2-}$. Where A is a relatively large size mono-, di- or tri-valentcation in 12-coordination site such as Na+ , K+ , Ba2+, Ca2+, Sr2+, Pb2+, Bi3+, etc. B is a small size, highly charged tera-, penta- or hexavalent cation in the octahedral coordination site of pseudo-perovskite unit and the site is generally occupied by Ti^{4+}, Ta^{5+}, Nb^{5+}, V^{5+}, W^{6+}, etc and n=1 to 5. So Some typical examples of BLSFs are: Bi2WO6 (n = 1), SrBi2Ta2O9 (n = 2), Bi4Ti3O12 (n = 3), MBi4Ti4O15 (M = Ca, Sr, Pb, Ba) (n = 4) and $Ba_2Bi4Ti_5O_{18}$ (n = 5), etc. Ferroelectricity mainly arises in these materials due to the perovskite blocks of BLSF , such as [21]:

A) Tilting of the oxygen octahedral around the a-axis

B) Tilting of the oxygen octahedral around the c-axis

C) A shift of A and/or B-cations along the polar axis [17, 18].

Bi_2O_2 layers perform the function of an insulating layer and controls the electrical response such as electrical conductivity, band gap, etc. of the compound [22].

Among the stated BLSF compounds the four layer SrBi4Ti4O15 (SBT),CaBi4Ti4O15 (CBT),and BaBi4Ti4O15(BBT) attracted much attention because of their low operating voltage, fast switching speed, negligible fatigue up to 10^{12} switching cycles[19], excellent retention characteristics, and low leakage current density, Large remnant polarization, low coercive field, and high Curie temperature These properties makes the systems to be used in ferroelectric random access memory (FRAM and high temperature sensor application)[23]. These physical properties of these ceramics are greatly affected by the characteristics of the powder, such as particle size, morphology, purity, and chemical composition, method of preparation. So various researchers had attempt to prepare these oxides in different technique. However, the wet chemical techniques, sol gel, and hydrothermal and colloid emulsions are time consuming and involve highly unstable alkoxides and it is difficult to maintain reaction conditions. Among them one of the well-known method is the solid-state reaction method with the expectation that it can become a potential candidate for ferroelectric material.

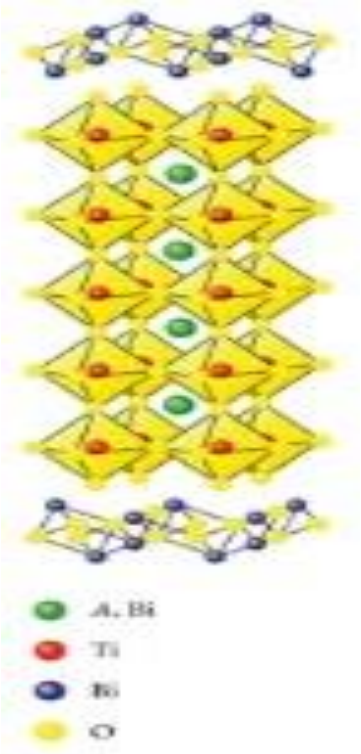

Structure of BLSF [24]

In the present report we are synthesis the SBT, BBT,CBT ceramic by solid-state reaction route and characterise by different tech. The structural study is done by the X-ray diffraction (XRD).The mic.

The phase transition study was done by temperature-dependent dielectric study. The ferroelectric property was confirmed by measuring the P-E loop tracer.

CHAPTER – 3

Experimental Procedure

Experimental Procedure:

In the present investigation $SrBi_4Ti_4O_{15}$(SBT), $BaBi_4Ti_4O15$ (BBT), and $CaBiTi_4O_{15}$ (CBT) synthesized by the process of ball milling. The compounds $SrCO_3$, $BaCO_3$, $CaCO_3$, Bi_2O_3 and TiO_2 were weighed in desired stoichiometric amounts. The resultant mixer was then set for Ball Milling using Zr balls for a time span of 24hrs in acetone medium. The dried power was then taken for manual grinding for 1hr using mortar pestle. The powdered sample was then carried for calcination at 900°c for 3h for SBT and 1000°c for 2h for BBT and CBT respectively. The calcined powers were then taken for characterization for XRD, UV and FTIR. The powder samples were mixed with 3% PVA as binder and grinded till the powder dries out. The pellets were made at about 60 Kg/cm^2 pressure for 5 minutes and sintered at respective temperatures(i.e. 1000°c, 1100°c and 1100°c) for SBT, BBT and CBT. A JEOL scanning electron microscope (model JSM-840) was used to study the microstructure of the sintered pellet. Before electrical property measurement, the pellets were coated with silver electrode. The temperature dependent dielectric measurement were carried out by Wayner kerr 6500 LCR meter over a wide range of temperature from room temperature to 800°C for SBT and CBT and 500°C for BBT. The ferroelectric hysteresis

loops were measured by standard ferroelectric analyzer.

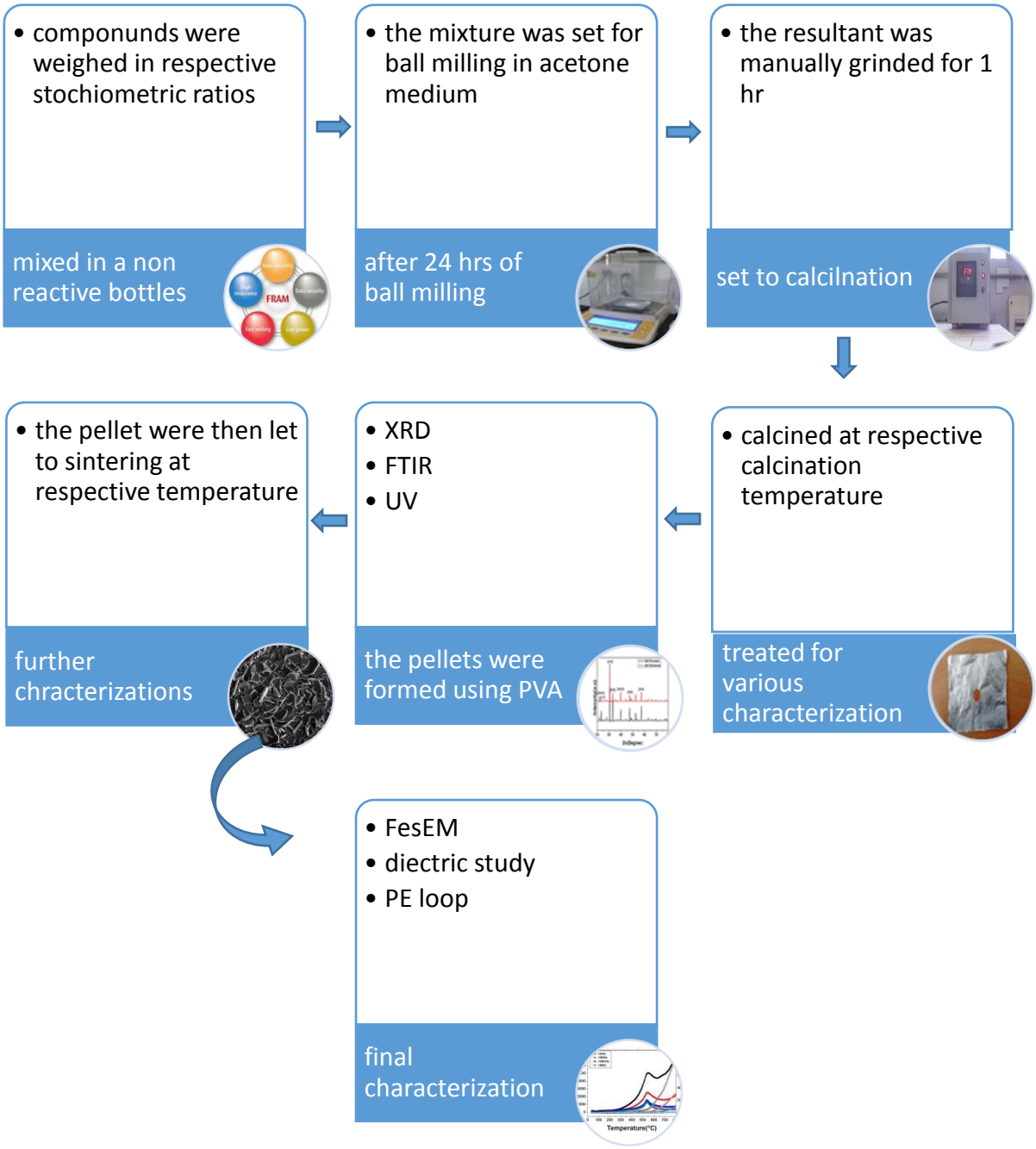

Flowchart of the experimental procedure

Chapter 4

Characterization Techniques

4.1) X-Ray Diffraction

Structural analysis SBT, BBT and CBT was performed in an X-ray diffractometer (XRD) using CuK_α (λ=1.54A^o). Nanocrystaline sizes were estimated from XRD measurements in our experiment. XRD statistically gives structural information about the whole sample and the calculation of the Debye Sherrer's equation [25] is the ideal tool to be associated with structural studies. The theory behind the X-Ray diffraction technique is explained below.

When an energetic electron knocks out another electron from the inner orbital, the outer electron makes a transition to fill the vacancy this leads to the creation of the characteristic spectra in the X-ray. While interacting with the electron of inner orbital the energy electron continuously decreases its velocity with leads to the formation of continuous spectra.

Bragg law given by[26] -

$$\mathbf{2d \sin\theta = n\lambda}$$

Where d is the interplanar separation, θ is the diffraction angle, n is the order of diffraction and λ is the wavelength of the incident x-rays. Therefore it is quite clear that the above consideration leads to the condition [27] –

$$\mathbf{n \leq 2d}$$

Since most of the crystal planes have d ~ 3 Å, therefore should not exceed 6 Å.

Below is the pictorial representation of Bragg's Law

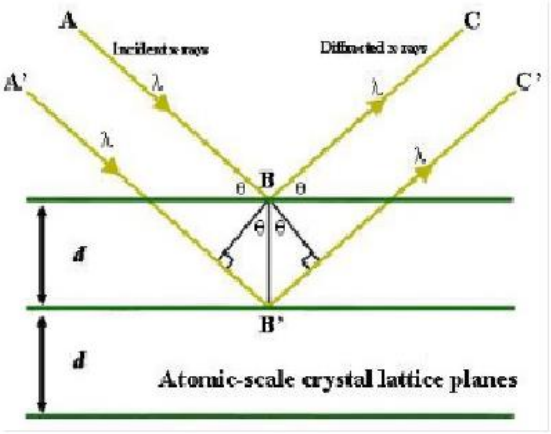

FIGURE 2: Pictorial representation of Bragg's Law

4.2) SEM

The scanning electron microscope (SEM) uses a focused beam of high-energy electrons to generate a range of signals at the surface of solid specimens. The signal that is backscattered or the secondary electrons are used to reveal information about the sample including external morphology (texture), chemical composition, and crystalline structure and orientation of materials making up the sample. EDS is attached to this instrument for element detection.

Scanning Electron Microscopy (SEM)

Instrumentation

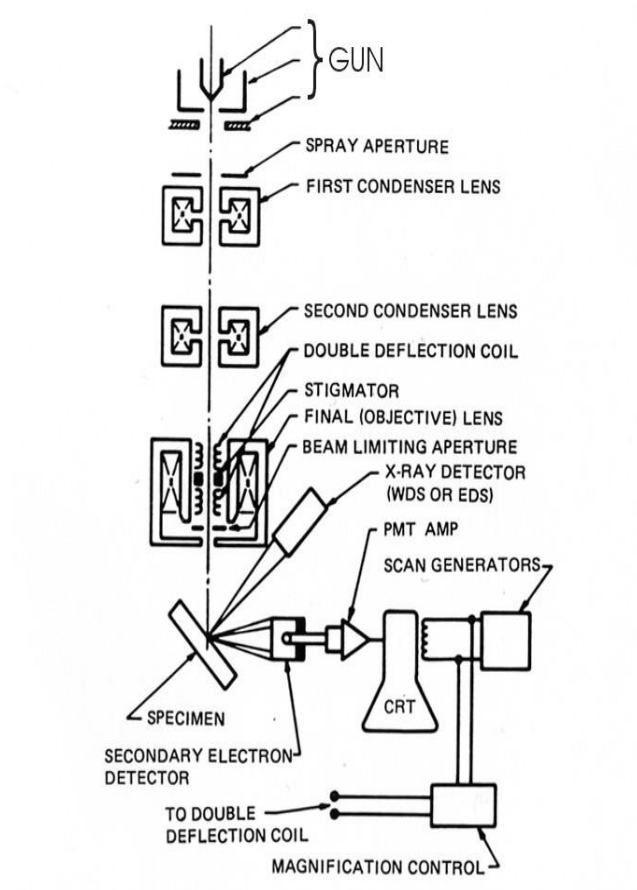

Essential components of all SEMs include the following [28]:

- Electron Source ("Gun")
- Electron Lenses
- Sample Stage
- Detectors for all signals of interest
- Display / Data output devices
- Infrastructure Requirements:
  - Power Supply
  - Vacuum System
  - Cooling system
  - Vibration-free floor
  - Room free of ambient magnetic and electric fields

SEMs always have a secondary electron

detector), and most have additional detectors. The specific capabilities of a particular instrument are critically dependent on which detectors it accommodates.

4.3) FTIR

FT-IR stands for Fourier Transform InfraRed, the preferred method of infrared spectroscopy. In infrared spectroscopy, IR radiation is passed through a sample. Some of the infrared radiation is absorbed by the sample and some of it is passed through (transmitted). The resulting spectrum represents the molecular absorption and transmission, creating a molecular fingerprint of the sample. Like a fingerprint no two unique molecular structures produce the same infrared spectrum. This makes infrared spectroscopy useful for several types of analysis.

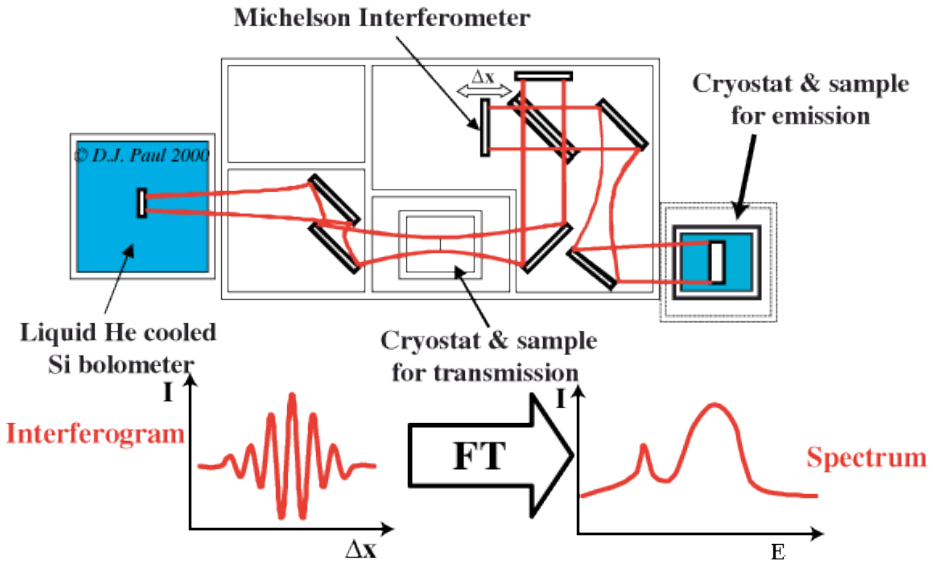

• It can identify unknown materials

• It can determine the quality or consistency of a sample

• It can determine the amount of components in a mixture

The normal instrumental process is as follows[29]:

1. The Source: Infrared energy is produced from a glowing black-body source.

2. The Interferometer: The beam enters the interferometer where the "spectral encrypting" takes place.

3. The Sample: The beam enters the sample compartment where it is transmitted through or reflected off of the surface of the sample, depending on the type of analysis being accomplished. This is where specific frequencies of energy, which are uniquely characteristic of the sample, are absorbed.

4. The Detector: The beam finally passes to the detector for final measurement. The detectors used are specially designed to measure the special interferogram signal.

5. The Computer: The measured signal is digitized and sent to the computer where the Fourier transformation takes place. The final infrared spectrum is then presented to the user for interpretation and any further manipulation.

4.4) UV-Visible spectroscopy

The band structure of a given semiconductor is very important in determining its potential utility. Consequently, an accurate knowledge of the band structure is critical.. The band gap of a material can be determined from its UV absorption spectrum. The term “band gap” refers to the energy difference between the top of the valence band to the bottom of the conduction band .

Electrons are able to jump from one band to another. In order for an electron to jump from a valence band to a conduction band, it requires a specific minimum amount of energy for the transition, called the band gap energy [30].

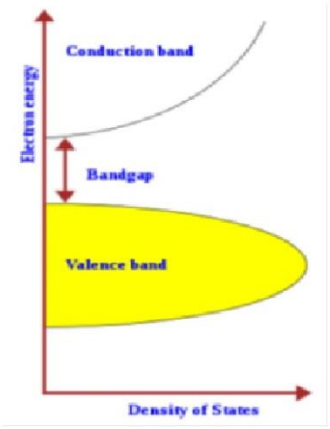

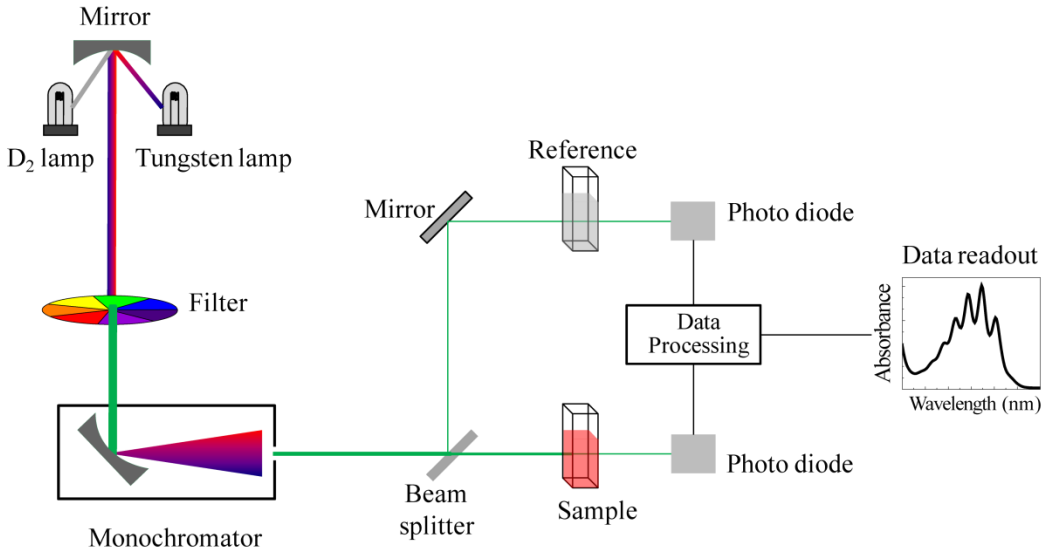

A schematic diagram of UV visible spectrometer

4.5) DIELECTRIC STUDY

When a dielectric is subjected to an electric field, a current flows. This total current flowing in a dielectric is made up of two parts:

(a) Conduction current

(b) Displacement current.

The displacement current is the elastic response of the dielectric material to the applied electric field. When the amplitude of the electric field is increased, the additional displacement gets stored within the dielectric as potential energy. As the amplitude of the electric field is decreased, the dielectric releases some amount of its stored energy as the displacement current. This displacement current can be separated into a vacuum contribution and the other part as resulting from the dielectric by the relation [31]:

$D = \varepsilon_o E + P$

where,

E is the electric field and P is the polarization of the dielectric. The capacitance of a dielectric capacitor arises due to dielectric polarization. Dielectric polarization may be described as the separation of bound

charges in a dielectric material into positive and negative charge entities when subjected to an electric field. There are different types of polarization occurring in a material. They are electronic, ionic, dipolar and space charge polarization [7]. Of these, electronic, ionic and dipolar polarizations are dependent on the bound charges of the material whereas space charge is concerned with the free charge. When the material is placed in an electric field, the electron cloud of the atom is displaced slightly with respect to the nuclei, causing electronic polarization. Ionic polarization is concerned with the motion of positive and negative charges in an electric field. Dipolar polarization also known as ion jump polarization is the preferential occupation of equivalent or near equivalent lattice sites on application of an external field. The free charges capable of migrating that are trapped in the interface of the material give rise to space charge polarization. The total polarization of a material is the sum of all the four polarization. The dielectric loss (tan δ) is the measure of energy dissipated in a dielectric on application of an electric field, which can be expressed as the ratio of resistive (loss) component of the current to the capacitive component of the current. When a varying voltage $V = V_o e^{i\omega t}$ is applied,[32] the total current in the dielectric is given by

$$I = \frac{dQ}{dt} = \frac{d(CV)}{dt} = jC\omega V = j\omega\varepsilon C_o V$$

where C_o is the capacitance in vacuum. As ε is a complex quantity ($\varepsilon = \varepsilon' - j\varepsilon''$), so I can be written as

$$I = j\omega(\varepsilon' - j\varepsilon'')C_o V = j\omega\varepsilon' C_o V + \omega\varepsilon'' C_o V = I_c + I_l$$

where Ic and I_l are the capacitive and loss component of the current, respectively. The total current (I) through the capacitor can be resolved into two components; the capacitive or charging current (Ic) is 90o out-of-phase with the voltage in an ideal capacitor, and the loss or conductive current (Il) is in-phase with the voltage [28]. However, in a real capacitor, the current lags behind the applied voltage by an angle δ. This is represented as the dielectric loss of the material which is the measure of energy dissipated in dielectric on application of an electric field. Fig shows the vector resolution of current (I) and the dielectric loss (tan δ) derived from it is given by,

$$tan\delta = \frac{I_c}{I_t} = \frac{\varepsilon'}{\varepsilon''}$$

4.6) PE loop

PE Loop tracer is designed for characterization of materials such as ferroelectrics. The system measures the hysteresis loops for these materials. The broad specifications and main features are listed here below[33]:

•There is a High voltage power supply with overload protection, Digital potentiometer.

•Input 220V Ac, Output 5KV Max Current 20mA, Programmable AC source variable frequency

•Programmable AC source fixed frequency 20Hz to 1kHz,.Current limiting circuit.

•ISA/USB Data acquisition hardware to collect samples from the unit.

•Temperature hardware for measuring the temperature of sample bath, Signal conditioning hardware with unity gain amplifier.

•Signal conditioning hardware with unity gain amplifier, Analogue to digital converter hardware.

•Integrator selector (for selection of internal reference capacitor and resistance)

•Sample holder Heater 400 Dec C Ramp controller, Temperature measurement hardware.

•Minimum Sample Resistance 200 K Ohm, Software for measurement data recording and plotting.

•100ml silicon oil for immersion of the sample

CHAPTER – 5

Results and discussion

RESULTS AND DISCUSSION

5.1) XRD:

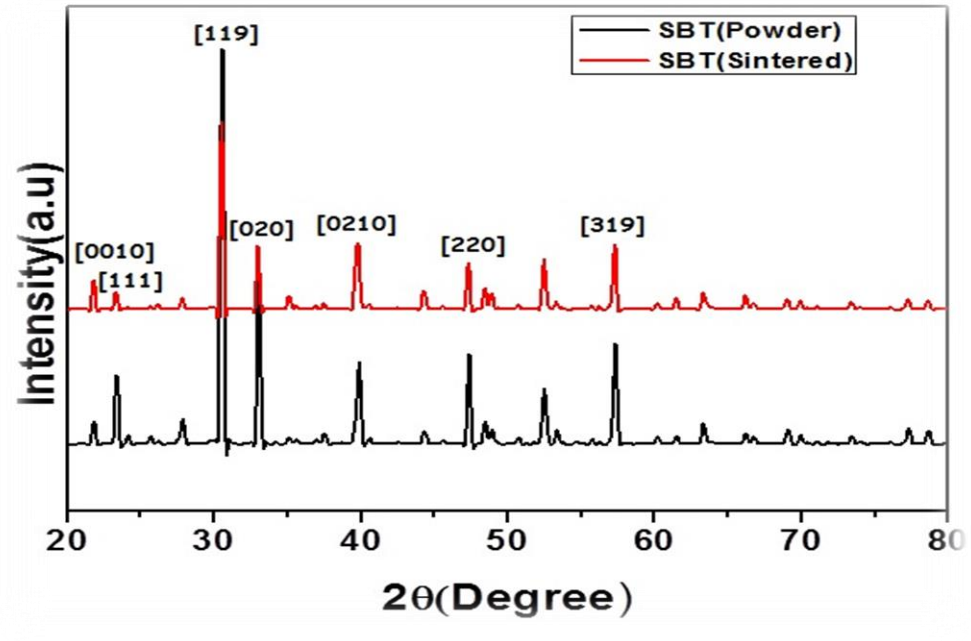

Fig – 1 (XRD of SBT pellet and powder)

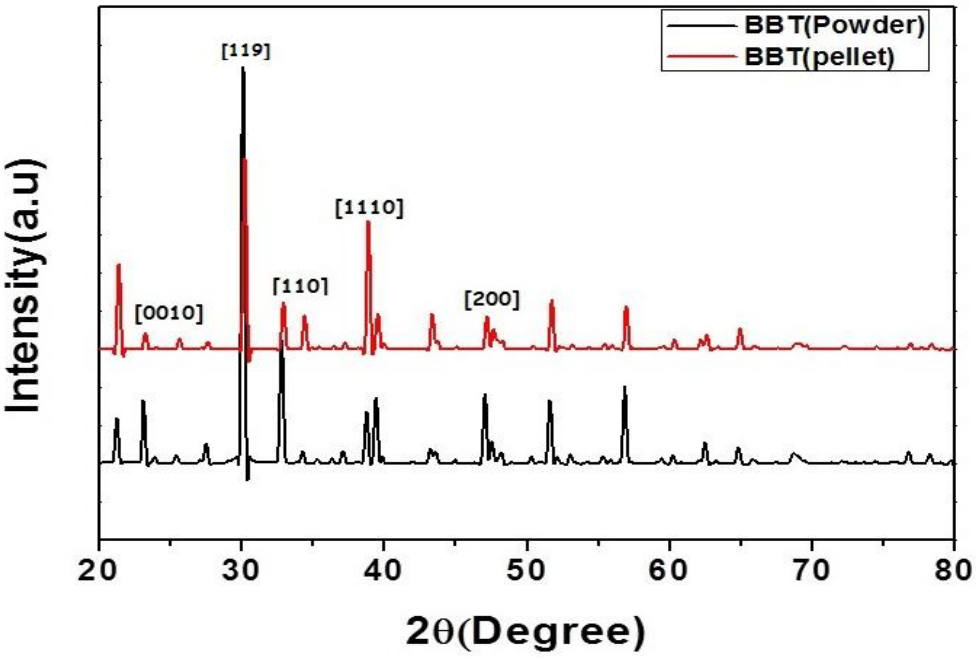

Fig – 2 (XRD of BBT pellet and powder)

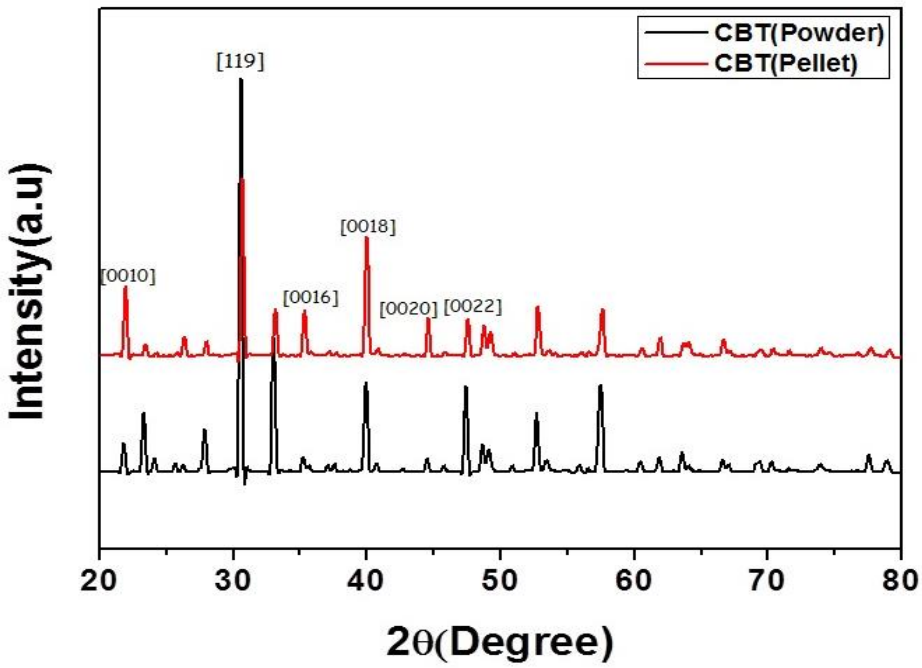

Fig – 3 (XRD of CBT pellet and powder)

Figures 1–3 shows the room temperature powder XRD patterns of SBT, and BBT and CBT ceramics recorded by using Cu *Kα* radiation. All The XRD pattern shows a single-phase and indexed according to the orthorhombic lattice structure, which is in well agreement with the standard pattern. Strong preferential growth is observed along (119).There is no evidence of the existence of any impurity phase detected.

The lattice parameters are found to be *a*=5.4507, *b*=5.4376, and *c*=40.9841 Å for SBT, *a*=5.443, *b*=5.432, and *c*=41.694 Å for BBT *a*=5.461, *b*=5.4235, and *c*=40.550 Å for CBT ceramic. These observed lattice parameters are in excellent agreement with those reported elsewhere. All the prepared ceramics are orthorhomboic at room temperature and transforms to tetragonal at high temperature.

The width of the peaks is small, indicating a good crystallization state with a large grain size. Assuming a homogeneous strain across crystallites, the size of microcrystallites can be estimated from the full width half maximum (FWHM) values of diffraction peaks. An average crystallite size

could be obtained using the Scherrer formula [22] for crystallite size broadening of diffraction peaks:

$$D = \frac{0.94\lambda}{\beta \cos\theta},$$

Where λ is the X-ray wavelength, Θ the Bragg angle and β the FWHM of the diffraction peak. Typical value of 6.91 nm crystallite size has been estimated from (119) diffraction peak.

Using the Williamson Hall equation [25]:

$$\beta\cos\theta = 4\varepsilon\sin\theta + \frac{K\lambda}{D}$$

Where,

β = FWHM (full width half maximum)

Ɛ = microstrain

θ = angle in the intensity pattern

λ = wavelength of Cu Kα (0.154nm)

D = crystalline size

K = constant treated as 0.94

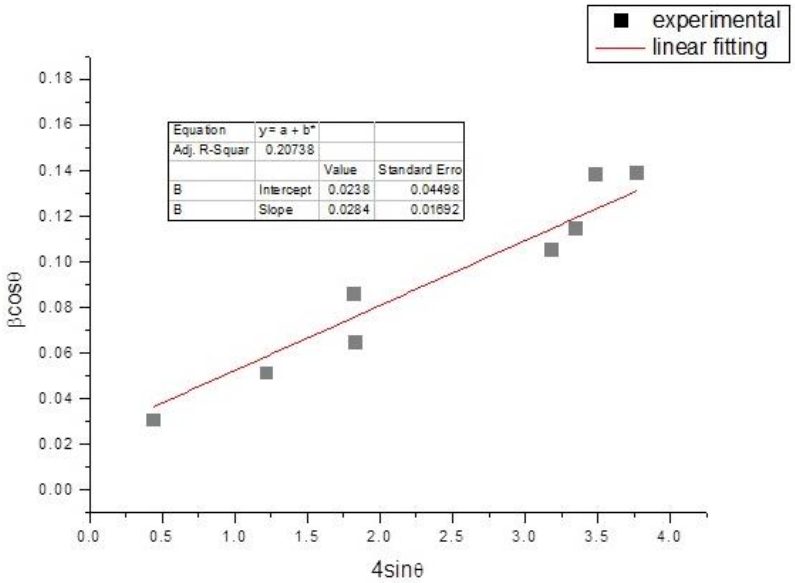

Fig – 4 (WH plot of SBT)

Graphically the crystalline size was calculated from the intercept of the WH plot as 6.02nm

The microstrain was calculated from the slope as 0.0284 x 10^{-3}. The average dislocation density can be calculated as 0.027 x 10^{12} lines/m^2.

Using the Scherrer's equation and WH equation the crystalline size , microstrain and the average dislocation density was calculated to be 6.91nm, 0.02579 x 10^{-3} and 0.0209 x 10^{12} lines/m^2, which is in good agreement with graphical value.

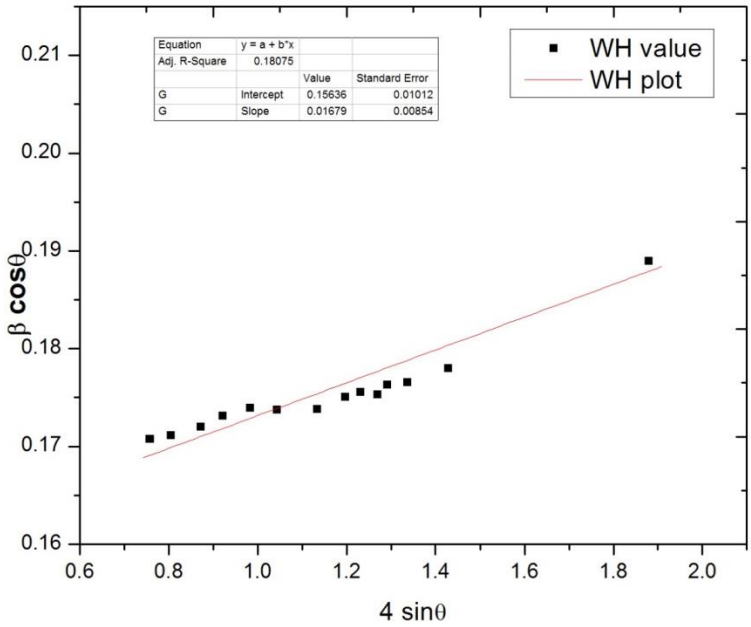

Fig – 5 (WH plot of BBT)

Similarly analysing WH plot the crystalline size, microstrain and the dislocation density can be calculated for BBT as 9.258A^{o} , The microstrain can be calculated as 0.0167 x 10^{-3} and the dislocation density is 0.0117x10^{12} lines/m^2.

Using the Sherrer's formula particle size calculated ss 9.33nm. The dislocation density as 0.0114 x10^{12} lines/m^2 and from the WH equation the microstrain is calculated as 0.015 x 10^{-3}.

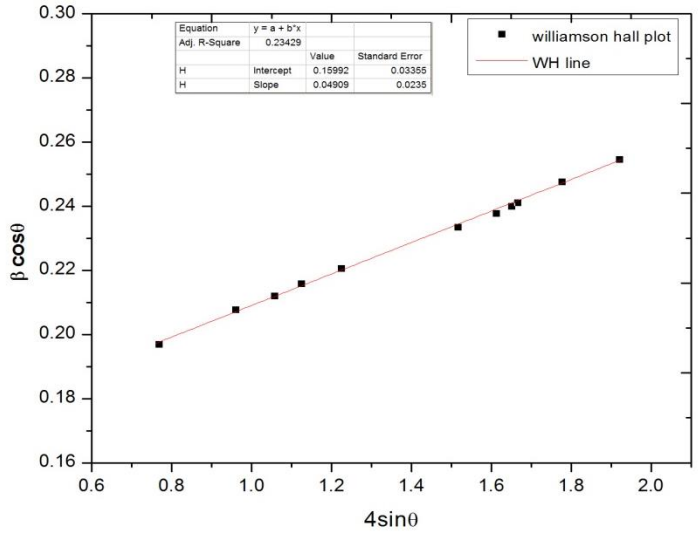

Fig – 6 (WH plot of CBT)

The microstrain can be calculated as 0.049 x 10^{-3} and from the intercept crystalline size is calculated as 9.09nm. the dislocation density as 0.01209 x 10^{12} lines/m^2.

Using the Sherrer's formula particle size calculated ss 9.03nm. The dislocation density as 0.0122x10^{12} lines/m^2 and from the WH equation the microstrain is calculated as 0.046 x 10^{-3}.

5.2) SEM:

Figure 7 shows the SEM micrograph of different ceramics prepared through solid state reaction route. The figure shows a platelike grain structure. which is the general characteristics of bismuth layer structure. It is also found from the micrograph that the grains of different sizes are homogeneously distributed. The Grain size are calculated which is 1.73µm for SBT and 1.67µm for BBT and 1.62µm for CBT.

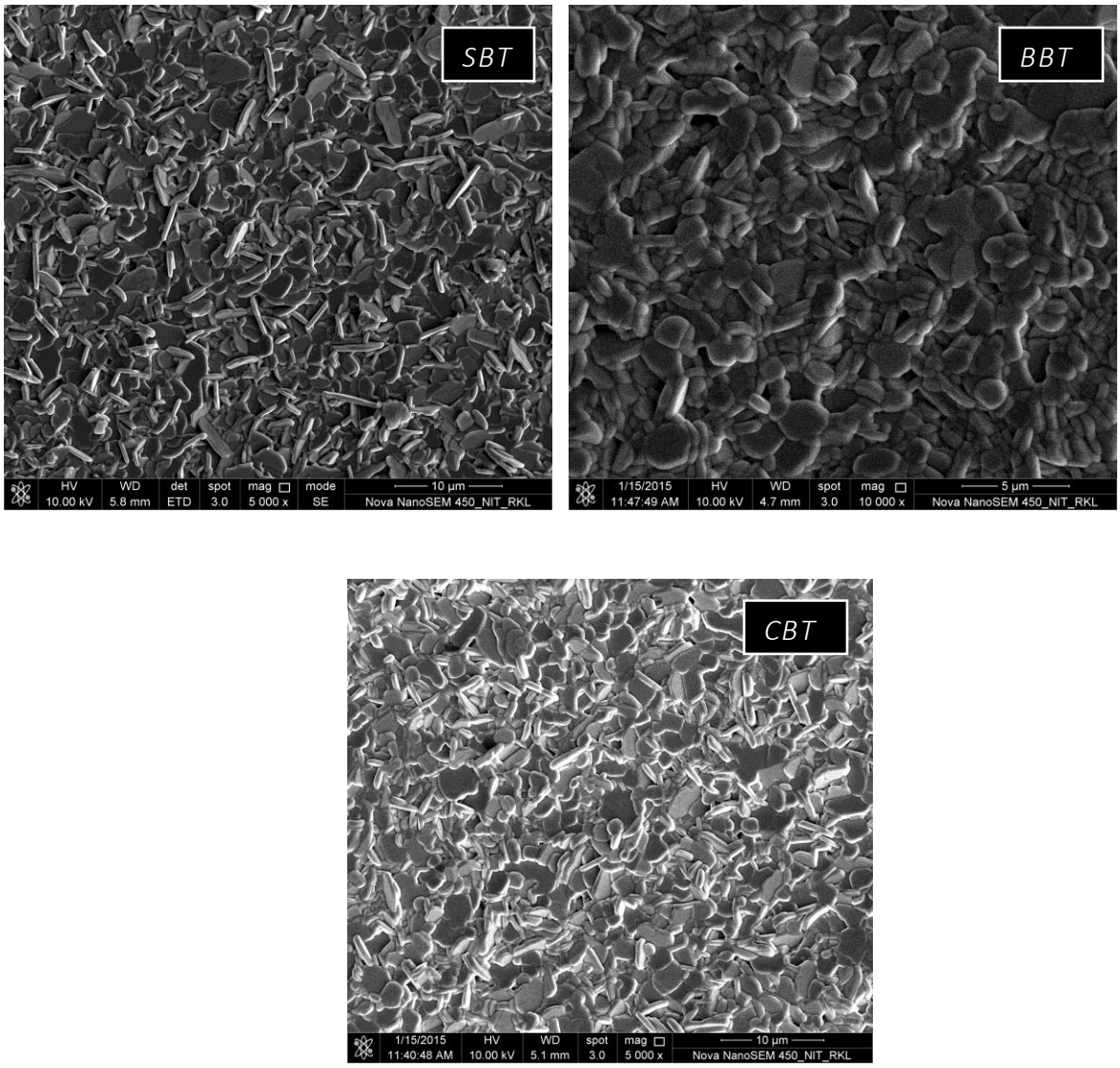

Fig – 7 (The SEM micrographs of SBT, BBT and CBT (clockwise))

5.3) FTIR

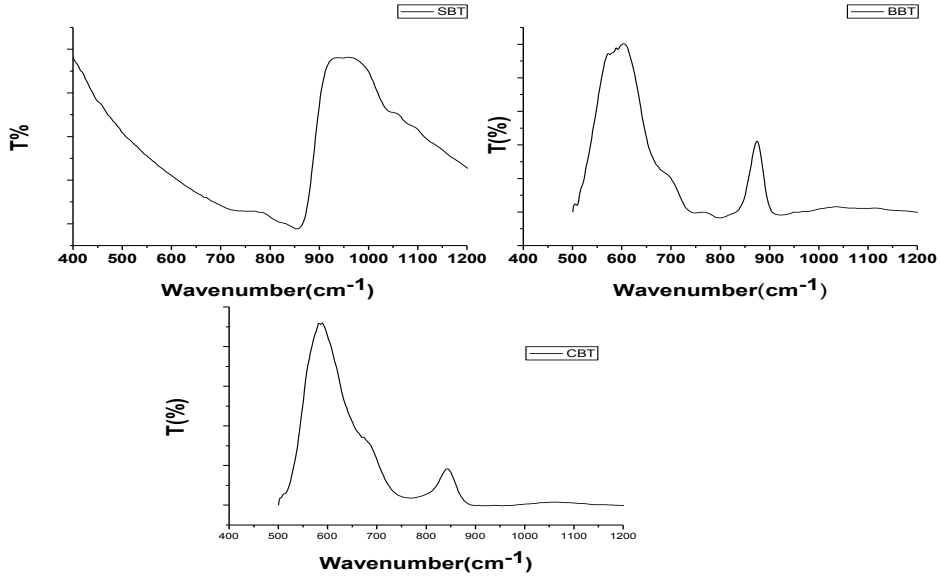

Fig -8 (FTIR analysis for SBT, BBT and CBT)

Fourier transform infrared spectra (FTIR) of SBT, BBT and CBT samples are shown in Fig. 5(a-c).The absorption band between at 800 $cm^{-1}$to 850cm^{-1} arises in all the prepared sample which is assigned to the vibrations arising from the strongly covalently bonded $(Bi_2O_3)^{2+}$ layers. The band in the range 580 cm^{-1} to 680 cm^{-1} were observed in the spectra of prepared BBT and CBT ceramic samples which is due to the Ti–O stretching vibration[13]. The stretching vibration is expected to occur at frequencies higher than the bending vibration, from the comparison of the change in potential energy due to repulsive forces between the ions in the two normal vibrations.

5.4) UV analysis

Band gap measurement:

$$\frac{K}{S} = \frac{(1 - R_\infty)^2}{2R_\infty} = F(R_\infty)$$

K-absorption coefficient

S- scattering co efficient.

Where $F(R_\infty)$ is remission or Kubelka–Munk (K–M) function. If we assume the scattering from the material remains constant for the entire wavelength range, the 'Kubelka-Munk function' is proportional to the absorption co-efficient (α).

For $K \rightarrow 0$ (no absorption), $R_\infty \rightarrow 1$ I.e. all light reflected.

Here F (R_∞) is remission or Kubelka–Munk (K–M) function. Instead of writing R_∞, R is suitable here. So $F(R) = (1-R)^2 / 2R$.

As the 'Kubelka-Munk function' is proportional to the absorption co-efficient (α),

$$\alpha h\nu = A\,[h\nu - E_g]^r$$

suggests that $[F(R)*h\nu]^{1/r} \propto [h\nu - E_g]$, Taking r = 2 for allowed direct band transition, $[F(R)*h\nu]^{1/2}$ vs. hν plot for the allowed indirect band gap measurement can be shown,.

Refractive index:

Experimentally measured optical band gap and the refractive index (n) are related by a relation given by Dimitrov and Sakka (1996). It is given by

$$(n^2-1)/(n^2+2) = 1-(E_g/20)^{1/2}.$$

Static dielectric constant and susceptibility measurement

Static or linear dielectric constant can be calculated using the relation given by

$$\epsilon_r = n^2$$

and the linear susceptibility (χ) related with dielectric constant as

$$\epsilon_r = 1 + \chi.$$

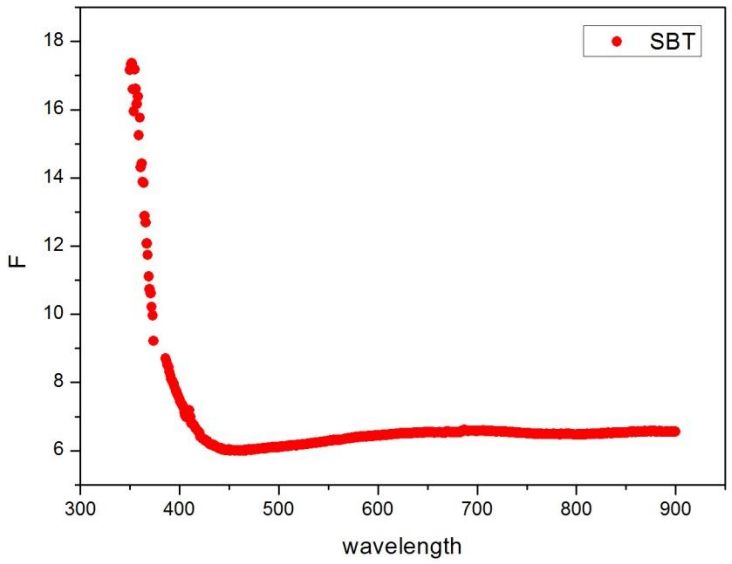

Fig – 9a (K-M function vs wavelength)

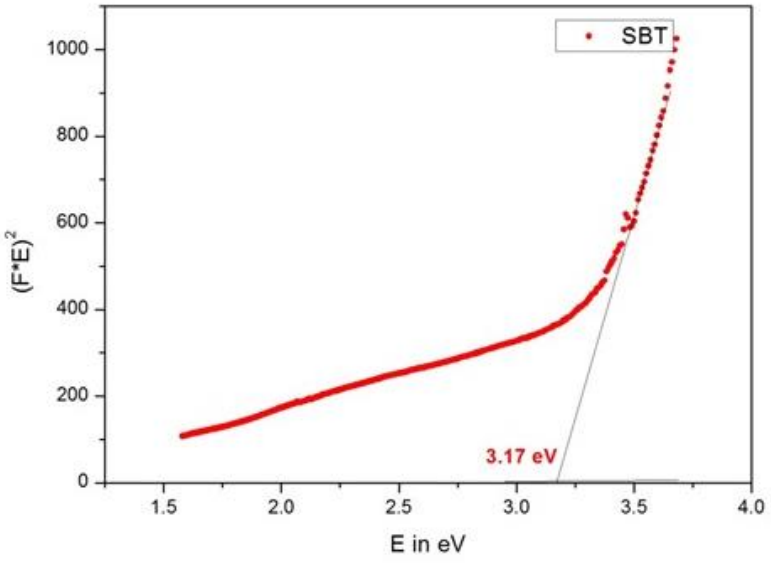

Fig 9b (direct band gap energy of SBT)

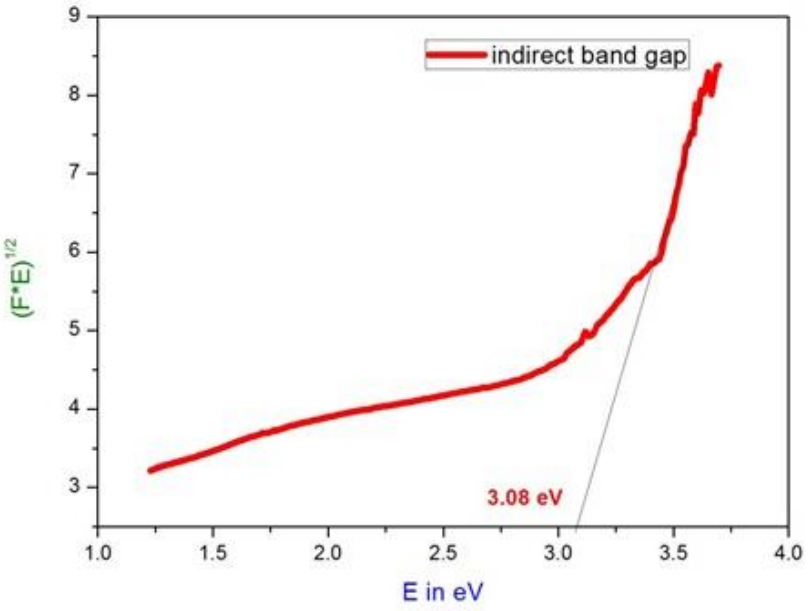

Fig – 9c (indirect band gap SBT)

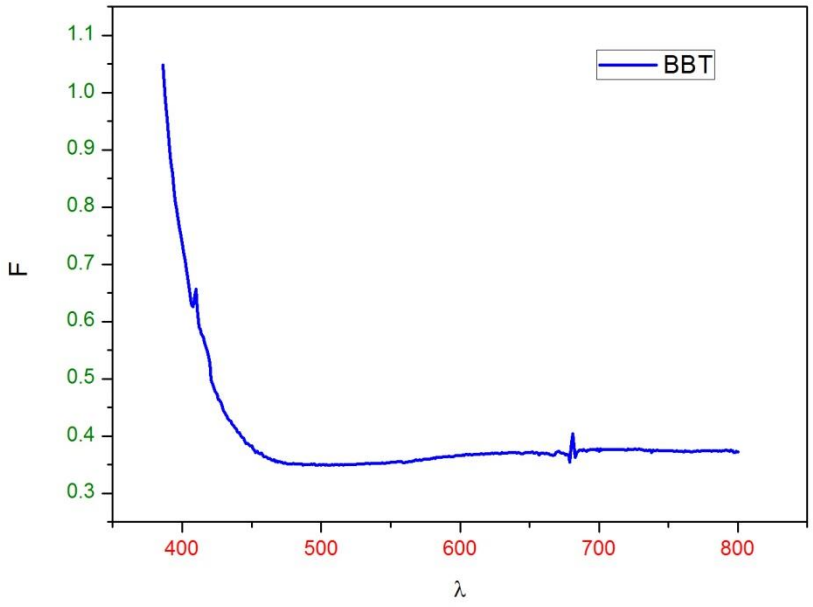

Fig - 9d (K-M function vs wavelength)

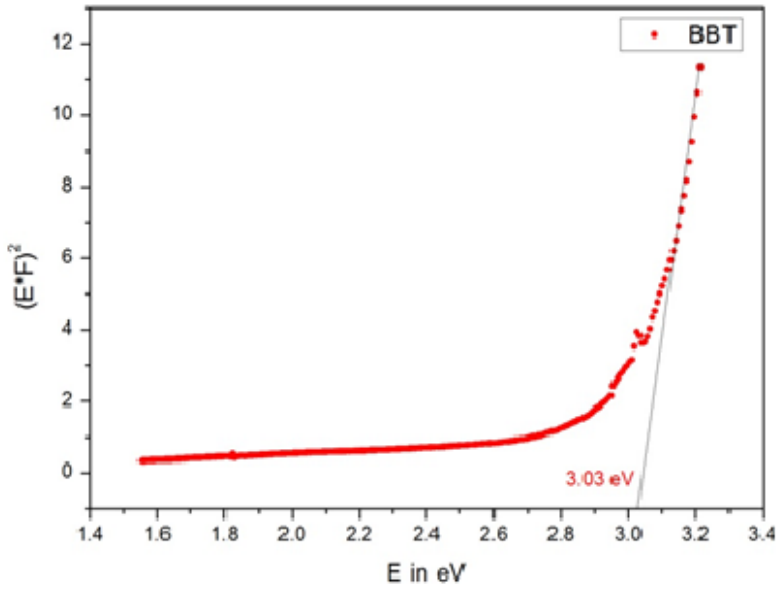

Fig – 9e (Direct band gap energy for BBT)

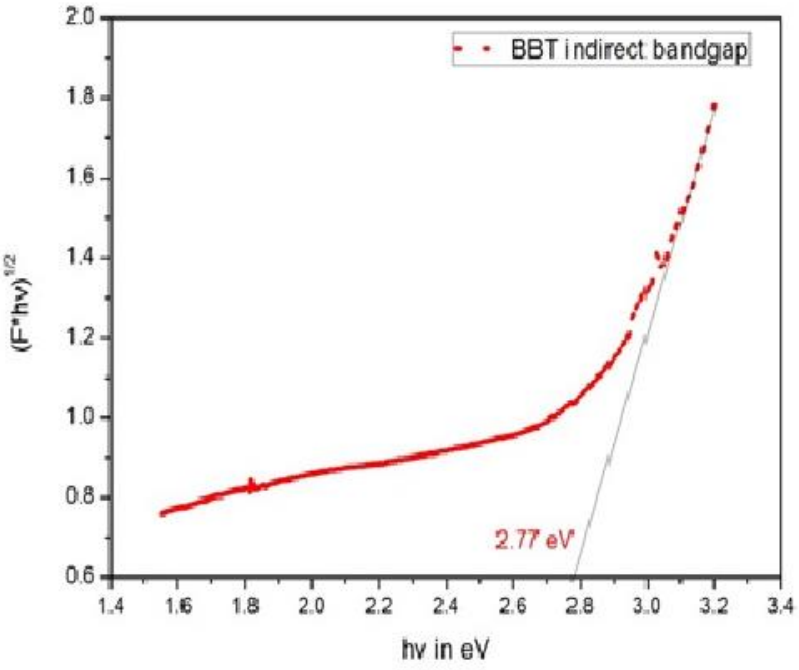

Fig – 9f (indirect band gap energy for BBT)

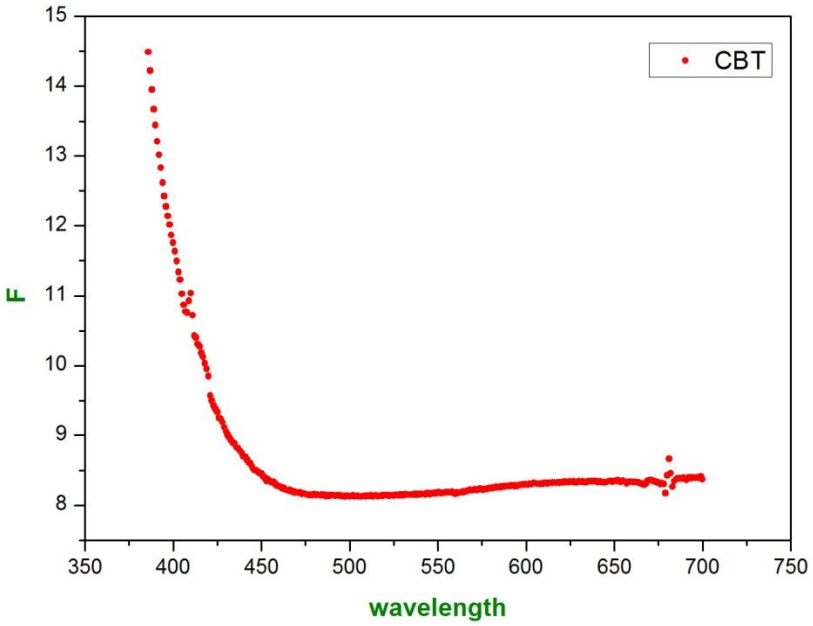

Fig – 9g (K-M function vs wavelength)

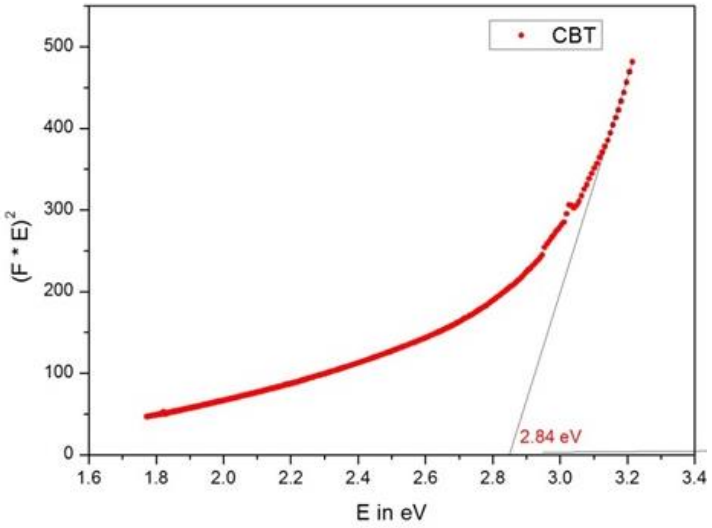

Fig – 9h (direct band gap energy for CBT)

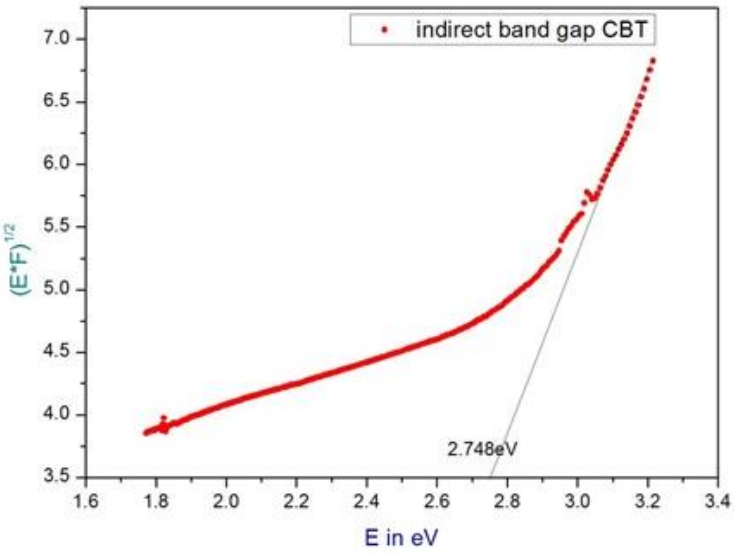

Fig 9i (indirect band gap energy for CBT)

sample	Eg (direct)	Eg (indirect)	ŋ	ε_r	χ
SBT	**3.17 eV**	**3.08eV**	**2.352**	**5.535**	**4.535**
BBT	**3.03eV**	**2.77eV**	**2.389**	**5.707**	**4.707**
CBT	**2.84eV**	**2.74eV**	**2.441**	**5.961**	**4.961**

5.5)Dielectric Analysis:

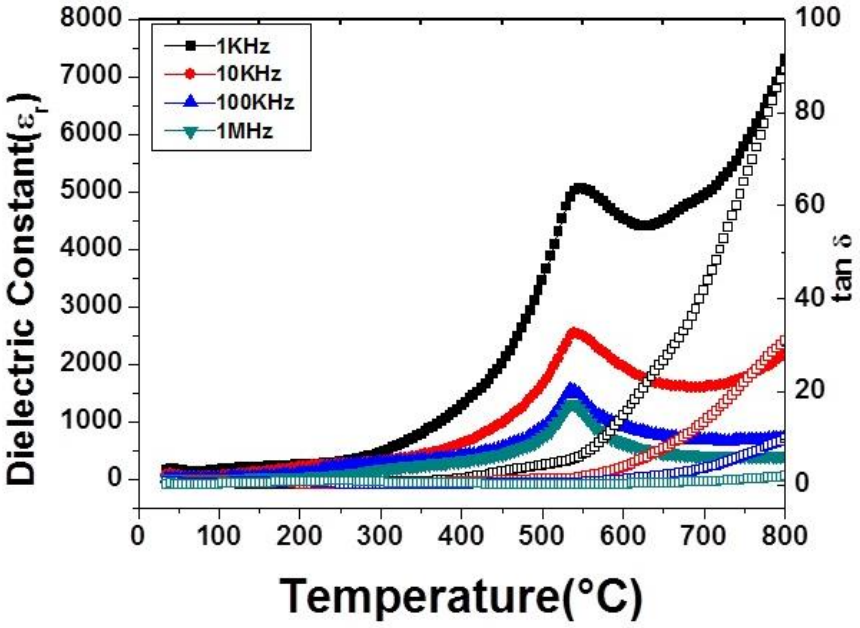

Fig - 10a

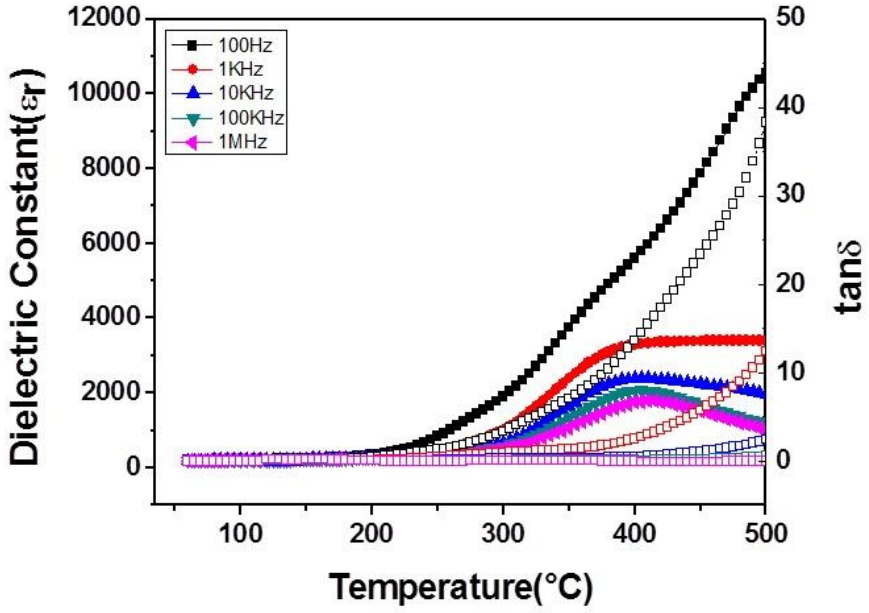

Fig – 10b

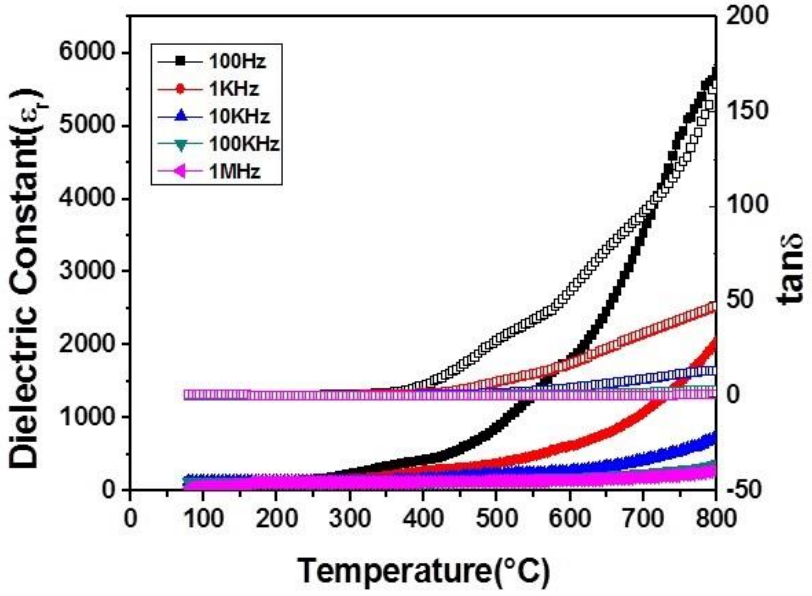

Fig – 10c

Figures 10a, 10b and 10c shows the temperature dependent dielectric properties permittivity and dielectric loss of ceramics in a five fixed frequency. It was found that the compounds SBT and CBT (Figures 10a and 10c) have frequency independent transition temperatures at 525 °C and 787°C respectively, indicating the occurrence of normal ferroelectric–paraelectric phase transitions. Above the transition temperature permittivity follows the Curie–Weiss law. For the BBT compound the dielectric anomaly is quite broad. This compound exhibits diffuse dielectric constant anomalies around Tm.

The T_c of the BBT specimen is about 400K. Moreover, the maximum in dielectric constant is diffusive and strong dispersion of dielectric maximum temperature (T_m) with frequency. The dielectric maximum shifts towards higher temperatures with increase in frequency which signifies the relaxor behavior of the present ceramics.

The dielectric loss (tan d) is very low and almost constant from room temperature to 400°C in all the prepared SBT, BBT and CBT ceramics and thereafter increases. The higher value of dielectric loss (tanδ) at high temperatures may be due to transport of ions with the higher thermal energy and also some defects in the samples. Also it maybe, at higher temperature the conductivity begins to dominate, which in turn is responsible for the rise in tanδ.

5.6) P-E Loop:

The ferroelectric behaviour of all the prepared ceramic are studied by room-temperature ferroelectric hysteresis loop with three different field which is shown in figure. The loops are far from saturation due to limitations of the experimental setup.

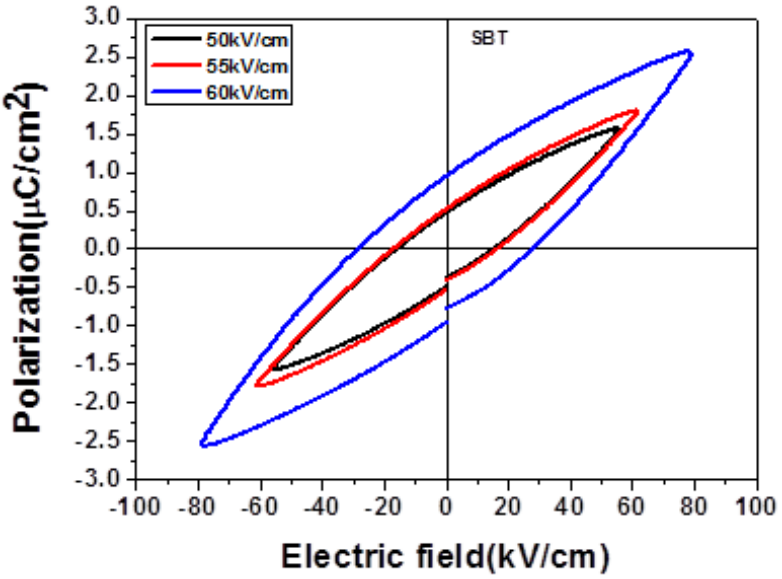

Fig 11a (PE loop for SBT)

Potential (kV/cm)	Ps (μC/cm^2)	Pr (μC/cm^2)	Ec (kV/cm)
60	2.554	0.95	27.604
55	1.7903	0.522	16.118
50	1.564	0.475	14.99

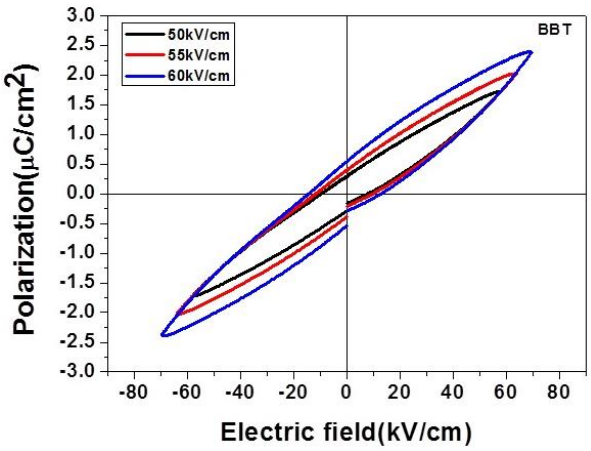

Fig – 11b (PE loop for BBT)

Potential (kV/cm)	Ps (μC/cm^2)	Pr (μC/cm^2)	Ec (kV/cm)
60	2.385	0.541	12.963
55	2.019	0.388	9.983
50	1.718	0.295	7.864

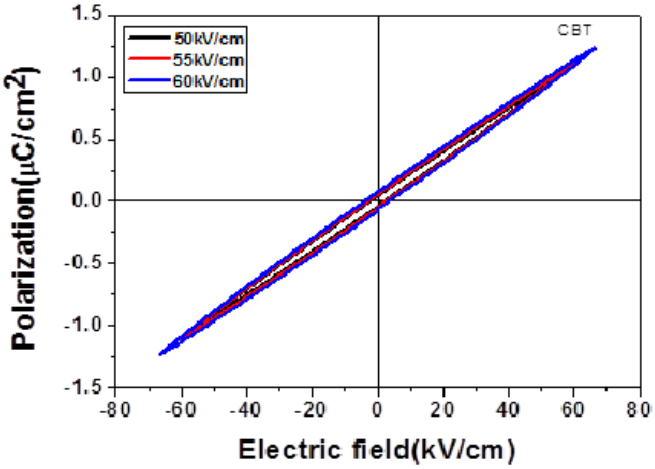

Fig – 11c (PE Loop for CBT)

Potential (kV/cm)	Ps (μC/cm^2)	Pr (μC/cm^2)	Ec (kV/cm)
60	1.227	0.074	3.238
55	1.114	0.056	2.487
50	1.008	0.044	1.857

Chapter - 6

Conclusions

Conclusions

In summary we have presented the structural, electrical and optical properties of SBT, BBT and CBT ceramics. Single phase Bi layered perovskite structure was confirmed by the XRD analysis. The crystalline size, dislocation density and microstrain was calculated using the Williamson Hall equation. Plate like grains morphology were observed in all three ceramics which is a general characteristic of Bi layer structure ferroelectric. The bonding nature was observed using FTIR. The direct band gap energy for SBT, BBT and CBT was calculated as 3.17, 3.03 and 2.84 eV respectively whereas the indirect band gap was calculated as 3.08, 2.77 and 2.74 eV. The static dielctric constant , refractive index and susceptibility was also calculated using the UV spectroscopy. From the dielectric study we observe SBT and CBT to be normal ferroelectric and BBT to relaxor ferroelectric. The ferroelectric property was conformed from the PE Loop tracer.

REFERENCES

[1] O. Auciello, Integr. Ferroelectr. 15 (1997) 211.

[2] T. Hase, T. Noguchi, Integr. Ferroelectr. 16 (1997) 29.

[3] S. Kim, M. Miyayama, H. Yanagida, J. Ceram. Soc. Jpn. 102 (1994) 722.

[4] S. Kim, M. Miyayama, H. Yanagida, J. Ceram. Soc. Jpn. 103 (1995) 315.

[5] B.H. Park, B.S. Kang, S.D. Bu, T.W. Noh, J. Lee, W. Joe, Nature 401 (1999) 682.

[6] S. Obregon Alfaro, A. Martinez-de la Cruz, Applied Catalysis A: General 383 (2010) 128.

[7] H. Yan, H. Zang, M.J. Reece, X. Dong, Appl. Phys. Lett. 87 (2005) 082911.

[8] F. Chu, D. Damjanovic, O. Steiner, N. Setter, J. Am. Ceram. Soc. 78 (1995) 3142.

[9] H.S. Shulman, M. Testorf, D. Damjanovic, N. Setter, J. Am. Ceram. Soc. 79 (1996) 3124.

[10] J.A. Horn, S.C. Zhang, U. Selvaraj, G.L. Messing, S. Trolier-McKinstry, J. Am. Ceram. Soc. 82 (1999) 921.

[11] S.K. Rout, E. Sinha, A. Hussain, J.S. Lee, C.W. Ahn, I.W. Kim, S.I. Woo, J. Appl. Phys. 105 (2009) 024105.

[12] J.C .Burfoot and W. Taylor, McMillan Press Ltd. (1971)

[13] J.C .B urfolk and W .Taylor POLAR Dielectrics and the Applications M acm illan Press Ltd(1971).

[14] S.A .A m in, R.Guo, A .S.Bhalla, Ceram, Trans 106, 157 (2000).

[15]. Chris Binns, Introduction to nanoscience and nanotechnology, WILEY publication (2010).

[16]. D. Paul Joseph and C. Venkateswaran, Journal of Atomic, Molecular, and Optical Physics,(2011).

[17] H. Yan, C. Li, J. Zhou, W. Zhu, L. He, Y. Song, Jpn. J. Appl. Phys. 39 (2000) 6339.

[18] A.Z. Sim~oes, M.A. Ramı´rez, A.H.M. Gonzalez, C.S. Riccardi, A. Ries, A. Longo, J.A. Varela, J. Solid State Chem. 179 (2006) 2206.

[19] A.Z. Sim~oes, A.H. Gonzalez, C.S. Ricardi, M. Cantoni, M.A. Zaghete, B.D. Stojanovic, J.A. Varela, J. Eur. Ceram. Soc. 24 (2004) 1607.

[20] D.E. Clarck, D.C. Folz, J.K. West, Mater. Sci. Eng. A 287 (2000) 153.

[21] E. Vigil, L. Saadoun, X. Domenech, I. Zumeta, Thin Solid Films 365 (2000) 12.

[22] D. Keyson, D.P. Volanti, L.S. Cavalcante, A.Z. Sim~oes, I.A. Souza, J.S. Vasconcelos, J.A. Varela, E. Longo, J. Mater. Process. Technol. 189 (2007) 316.

[23] T. Watanabe, H. Funakubo, K. Saito, J. Mater. Res. 16 (2001) 303.

[24] K. Kato, K. Suzuki, K. Nishizawa, T. Miki, Appl. Phys. Lett. 78 (2001)

[25]. N. Pinna, X-Ray diffraction from nanocrystals, Progr Colloid Polym Sci Springer, 130: 29-32, (2005).

[26]. V. Petkov,T. Ohta,Y. Hou,and Y. Ren, J. Phys. Chem. C, 111:(714-20),(2007).

[27]. Hoffman, M., Martin, S., Choi, W., & Bahnemann, Chemical Review, 95:(69-96), (1995).

[28]. Daniel Fritsch, Heidemarie Schmidt, and Marius Grundmann. Appl. Phys. Lett., 88: 134104, (2006).

[29]. H. Ohno, et al.,. Science, 281: 951, (1998).

[30]. Vladimir A. Fonoberov, Khan A. Alim, and Alexander A. Balandin PhysRevB.,73:1103, (2006).

[31]. Hsin-Ming Cheng, Kuo-Feng Lin, Hsu-Cheng Hsu, and Wen-Feng Hsiehb, Appl Phys Lett, 88:261909, (2006).

[32]. Klug H, Alexander L. X-ray diffraction methods for poly-crystalline and amorphous materials, New York: John Wiley and Sons, (1954).

[33] C.A.P.de Araujo, J.D. Cuchiaro, L.D. McMillan, M. Scott, J.F. Scott, Nature 374 (1995) 627.